Dalton Transactions

PAPER

View Article Online
View Journal | View Issue

Cite this: *Dalton Trans.*, 2016, **45**, 1987

On the energetics of P–P bond dissociation of sterically strained tetraamino-diphosphanes†

M. Blum,[a] O. Puntigam,[a] S. Plebst,[a] F. Ehret,[a] J. Bender,[a] M. Nieger[b] and D. Gudat*[a]

Received 25th July 2015,
Accepted 27th August 2015

DOI: 10.1039/c5dt02854j

www.rsc.org/dalton

The homolytic P–P bond fission in a series of sterically congested tetraaminodiphosphanes $(R_2N)_2P–P(NR_2)_2$ ($\{\mathbf{4}\}_2$–$\{\mathbf{9}\}_2$, two of which were newly synthesized and fully characterized) into diaminophosphanyl radicals $(R_2N)_2P^\bullet$ (**4–9**) was monitored by VT EPR spectroscopy. Determination of the radical concentration from the EPR spectra permitted to calculate free dissociation energies ΔG^{295}_{Diss} as well as dissociation enthalpies ΔH_{Diss} and entropies ΔS_{Diss}, respectively. Large positive values of ΔG^{295}_{Diss} indicate that the degree of dissociation is in most cases low, and the concentration of persistent radicals – even if they are spectroscopically observable at ambient temperature – remains small. Appreciable dissociation was established only for the sterically highly congested acyclic derivative $\{\mathbf{9}\}_2$. Analysis of the trends in experimental data in connection with DFT studies indicate that radical formation is favoured by large entropy contributions and the energetic effect of structural relaxation (geometrical distortions and conformational changes in acyclic derivatives) in the radicals, and disfavoured by attractive dispersion forces. Comparison of the energetics of formation for CC-saturated N-heterocyclic diphosphanes and the 7π-radical **3c** indicates that the effect of energetic stabilization by π-electron delocalization in the latter is visible, but stands back behind those of steric and entropic contributions. Evaluation of spectroscopic and computational data indicates that diaminophosphanyl radicals exhibit, in contrast to aminophosphenium cations, no strong energetic preference for a planar arrangement of the $(R_2N)_2P$ unit.

Introduction

Kinetic stabilisation by sterically demanding substituents is an immensely useful concept which has played a key role in the advancement of modern organometallic and molecular inorganic chemistry and permitted the preparation of many new classes of isolable or persistent compounds.[1] A distinct example of previously unknown, kinetically stabilised species in main-group element chemistry are long-lived neutral pnictyl radicals $R_2E^\bullet$ (E = P, As).[2] The first specimens, **1** and **2** (Scheme 1), were generated in 1976 by Lappert *et al. via* reduction of chlorophosphane or chloroarsane precursors and identified as persistent radicals with half-lives $t_{1/2}$ > 1 month at 20 °C by EPR spectroscopy.[3] Building on this pioneering work, to date arsanyl and phosphanyl radicals with a wider selection of bulky alkyl, aryl or amino substituents have been characterized.[4,5]

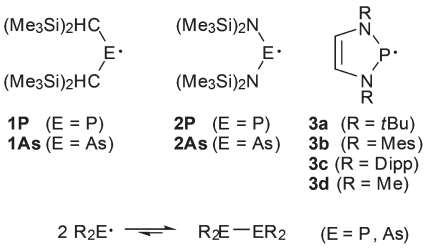

Scheme 1 Examples of persistent pnictyl radicals and a dimerization reaction under E–E bond formation.

Apart from some recent reports on stable phosphanyl radicals that were isolated and fully characterized in the crystalline state,[4f,h,i] the monomers exist generally only in the gas phase or in solution but are dimerized when solid.[4c,d,g,j,l,6] In several cases, temperature dependent equilibria between phosphanyl radicals and their dimers (Scheme 1) were detected spectroscopically in solution, and the observed prevalence of diphosphanes at low temperatures was interpreted as reflecting the

[a]*Institut für Anorganische Chemie, University of Stuttgart, Pfaffenwaldring 55, 70550 Stuttgart, Germany. E-mail: gudat@iac.uni-stuttgart.de*
[b]*Laboratory of Inorganic Chemistry, Dept. of Chemistry, University of Helsinki, P.O. Box 55, 00014 University of Helsinki, Finland*

† Electronic supplementary information (ESI) available: Experimental and simulated EPR spectra of **6–9**; plot of computed hyperfine couplings *vs.* skew angles; ^{1}H NMR spectra of **9**/$\{\mathbf{9}\}_2$; results and evaluation of VT EPR measurements; energies and coordinates of calculated molecular structures of radicals **4–9** and diphosphanes $\{\mathbf{4}\}_2$–$\{\mathbf{9}\}_2$; graphical representation of the structural relaxation; crystallographic data. CCDC 1414814 (**9_Cl**), 1414815 $\{\mathbf{8}\}_2$ and 1414816 $\{\mathbf{9}\}_2$. For ESI and crystallographic data in CIF or other electronic format see DOI: 10.1039/c5dt02854j

gain in enthalpy and the loss in entropy associated with the dimerization under P–P bond formation.[4c,e,g,j–l]

Detailed studies on the structural aspects of the dimerization of persistent pnictyl radicals were performed on **1** and the N-heterocyclic phosphanyl radical **3c**. Comparison of the molecular geometries of **1P**, **1As** (as determined by gas phase electron diffraction) and their dimers $\{(Me_3Si)_2CH\}_2E–E\{CH(SiMe_3)_2\}_2$ ($\{\mathbf{1P}\}_2$, E = P and $\{\mathbf{1As}\}_2$, E = As) revealed that the dimerization is accompanied by bond angle distortions in the alkyl groups and a reorientation of the $CH(SiMe_3)_2$ substituents in a R_2E unit from a *syn*,*syn*-conformation in the radicals to a *syn*,*anti*-conformation in the dimers. Backed by computational studies,[6,7] these changes were interpreted as indicating that the dimers in the crystal are loaded with a substantial amount of steric strain energy. The possibility to discharge the strain upon release of the molecule from the crystal lattice was seen as a strong driving force for the formation of monomers in solution or the gas phase, and led to a description of **1** as "Jack-in-the-box molecules".[6] In a recent computational analysis[8] of the dimerization of **1** it was emphasized that a realistic description of the energetics of this process requires also the consideration of dispersion forces: neglecting dispersion, the energy required for P–P bond homolysis was predicted insufficient to offset the stabilizing effect of structural relaxation in the radicals, and it is only due to the dispersive attraction between the radicals that dimer formation is energetically favoured.

A different source of energetic stabilization was discussed for the N-heterocyclic radicals **3**: based on a comparison of EPR hyperfine couplings to the ^{31}P and ^{14}N nuclei and computational evidence, Wright *et al.*[4g] concluded that the spin density is not mainly phosphorus-based as in other phosphanyl radicals, but rather delocalized over the heterocycle. They described these species consequently as 7π-radicals and postulated that their creation from the corresponding dimers should be facilitated by a combination of steric effects (repulsion between bulky substituents) and electronic stabilization by π-delocalization. In accord with this hypothesis, formation of persistent radicals **3c** from dissociation of the isolable dimer $\{\mathbf{3c}\}_2$ was observed at exceedingly mild conditions (room temperature) in solution,[4g] and an experimental evaluation of the energetics of the P–P bond homolysis of the dimer $\{\mathbf{3c}\}_2$ gave a dissociation enthalpy ΔH_{Diss} of 79 kJ mol^{-1},[4k] well below the average P–P bond enthalpy of 201 kJ mol^{-1}.[9] Computationally, the dissociation energies were greatly underestimated when dispersion forces were neglected (*cf.* an unrealistically low calculated dissociation energy of ≈3 kJ mol^{-1} for a *N*-Me substituted model dimer $\{\mathbf{3d}\}_2$),[4g] and overestimated when dispersion effects were included (*cf.* $\Delta H_{diss,calc}$ = 95.8 kJ mol^{-1} for $\{\mathbf{3d}\}_2$ and 129.9 kJ mol^{-1} for $\{\mathbf{3c}\}_2$ at the ωB97X-D/cc-pVDZ level of theory).[4k]

Summarizing the available knowledge on persistent phosphanyl (and arsanyl) radicals, it becomes clear that their common property is the stabilization against dimer formation or further reaction[4k] by sterically crowded substituents. The factors controlling this stabilization have been extensively studied for a few representatives (mainly **1**), but there are still many open questions which address, *e.g.*, the interplay of steric and electronic stabilizing effects in **3** and related cyclic or open diaminophosphanyl radicals. Improving our understanding of these factors is needed in order make better use of the still underdeveloped potential of the persistent radicals in synthesis, but also to deepen our insight into the reactivity and thermal stability of E–E-bonded frameworks, and the tuning of these qualities by steric strain. Furthermore, considering that the results of computational studies seem to depend strongly on the computational model applied,[4g,k,8] an experiment based research approach seems highly desirable in order to provide an unbiased reference point. We report here on the extension of a previous experimental study on the dissociation energetics of the diphosphane $\{\mathbf{3c}\}_2$ [4k] to include compounds featuring both N-heterocyclic ($\{\mathbf{4}\}_2$, $\{\mathbf{5}\}_2$, Scheme 2) and acyclic ($\{\mathbf{6}\}_2$–$\{\mathbf{9}\}_2$) molecular frameworks, and a discussion of the results in the light of computational studies.

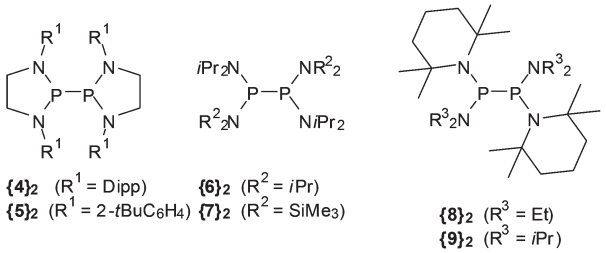

Scheme 2 Diphosphanes included in this study.

Results and discussion

Synthesis and characterization of sterically crowded tetraaminodiphosphanes and diaminophosphanyl radicals

Diphosphanes $\{\mathbf{4}\}_2$–$\{\mathbf{6}\}_2$ were prepared by reductive coupling of appropriate chlorophosphane precursors using previously published procedures.[4j,k,10] In case of $\{\mathbf{7}\}_2$, the reported protocol[4c] was modified by using sodium naphthalenide instead of potassium graphite as reducing agent. Finally, $\{\mathbf{8}\}_2$ and $\{\mathbf{9}\}_2$ were obtained analogously by reduction of the chlorophosphane precursors with magnesium or sodium (Scheme 3). Both new compounds were characterized by elemental analyses, spectral data, and single-crystal X-ray diffraction studies.‡

The individual molecules in crystalline $\{\mathbf{8}\}_2$ (Fig. 1) display crystallographic C_i-symmetry and exhibit therefore a staggered conformation in which both the two R_2P moieties as a whole and the two pairs of Et_2N and TMP substituents are mutually *trans* to each other. The nitrogen atoms adopt planar or near planar coordination geometries (sum of bond angles 360.0(4)° at N8 and 353.5(4)° at N2), and the coordination planes around these atoms are strongly twisted with respect to the

‡ Crystallographic data of the chlorophosphane **9_Cl** (the precursor of $\{\mathbf{9}\}_2$) are found in the ESI.†

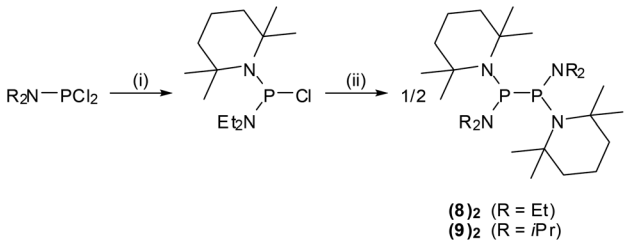

Scheme 3 Synthesis of the diphosphanes $\{\mathbf{8}\}_2$, $\{\mathbf{9}\}_2$. Reaction conditions: (i) 1 equiv. Li(tetramethylpiperidyl), THF, −78 °C to r.t.; (ii) excess Mg in THF ($\{\mathbf{8}\}_2$) or Na in hexane ($\{\mathbf{9}\}_2$), 3–7 h ultrasound at 48 °C.

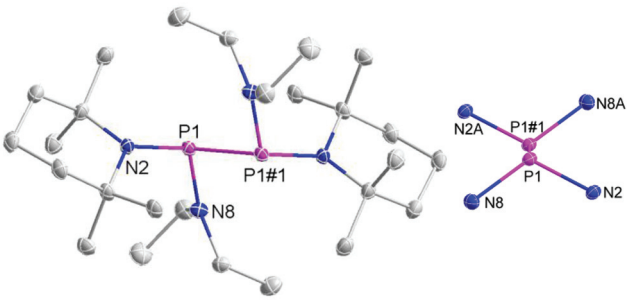

Fig. 1 Representation of the molecular structure of $\{\mathbf{8}\}_2$ in the crystal (left) and reduced plot of the central P_2N_4 skeleton (right). Thermal ellipsoids were drawn at 50% probability level, and H atoms were omitted for clarity. Selected bond lengths [Å]: P1–N8 1.7070(16), P1–N2 1.7395(15), P1–P1#1 2.2914(10).

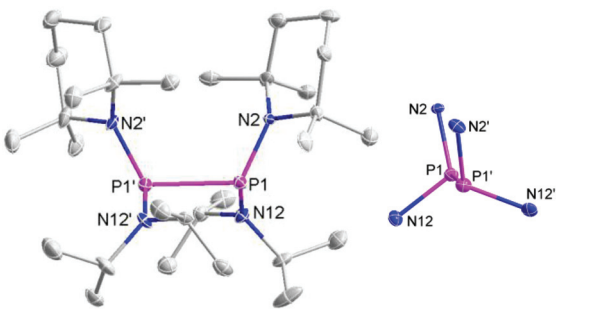

Fig. 2 Representation of the molecular structure of $\{\mathbf{9}\}_2$ in the crystal (left) and reduced plot of the central P_2N_4 skeleton (right). Thermal ellipsoids were drawn at 50% probability level, and H atoms were omitted for clarity. Selected bond lengths [Å]: P1–N12 1.727(5), P1–N2 1.738(5), P1–P1′ 2.357(2), P1′–N12′ 1.711(5), P1′–N2′ 1.740(5).

central NPN plane (skew angles§ 62° for the TMP and 80° for the Et_2N substituent). The molecules in crystalline $\{\mathbf{9}\}_2$ feature a *pseudo*-ecliptic alignment of the R_2P units (Fig. 2) in which the P–N bonds to the TMP substituents lie nearly in one plane (dihedral angle N(2)–P(1)–P(1′)–N(2′) 1.2(3)°) and the

§We define the skew angle as a dihedral angle ANPB where A and B are points on the normal vectors of the NPN and CNC/CNSi planes.

Table 1 P–P bond distances in strained diphosphanes

	P–P [Å]	Ref.
$\{\mathbf{1P}\}_2$	2.3103(7)	6*a*
$\{\mathbf{3c}\}_2$	2.3204(13)	4*k*
$\{\mathbf{4}\}_2$	2.3206(9)	4*j*
$\{\mathbf{5}\}_2$	2.270(2)	4*l*
$\{\mathbf{6}\}_2$	2.2988(8)[a]	11
$\{\mathbf{7}\}_2$	2.291(4)	4*d*
$\{\mathbf{8}\}_2$	2.2914(10)	This work
$\{\mathbf{9}\}_2$	2.357(2)	This work

[a] The disordered crystal contains a second unit with a distance 2.3013(13) Å.

piperidine rings are adjacent to each other. The resulting arrangement comes close to C_2-symmetry. As in $\{\mathbf{8}\}_2$, the coordination geometry at the nitrogen atoms is quasi-planar (sum of bond angles 357.0(9)–359.2(9)°). The skew angles between the NPN unit and the iPr_2N-substituent of *ca.* 83° are similar as in $\{\mathbf{8}\}_2$ whereas the skew of the TMP ring is less pronounced (skew angles *ca.* 53°).

The P–P distance in $\{\mathbf{8}\}_2$ falls into the range known for other strained symmetrical diphosphanes (Table 1) whereas that in $\{\mathbf{9}\}_2$ exceeds even the longest distances reported so far (2.320–2.321 Å in $\{\mathbf{3c}\}_2$ and $\{\mathbf{4}\}_2$)[4j,k] by more than 3 pm. A reasonable explanation for the extreme bond lengthening may be seen in the *pseudo*-ecliptic conformation which is most likely enforced by the steric requirements of the substituents and maximizes the Pauli-repulsion between P–N bonds and lone-pairs¶ at adjacent phosphorus atoms.

The ^{31}P spectra of $\{\mathbf{8}\}_2$ display two singlets with slightly unequal intensity, and the ^1H and ^{13}C NMR spectra contain two sets of signals of Et_2N and tetramethylpiperidyl (TMP) substituents. Similar features had also been observed for $\{\mathbf{7}\}_2$ [4c] and indicate the presence of a mixture of *meso*- and *rac*-diastereomers with different stereochemical configuration at the phosphorus atoms in solution. A ^{31}P NMR spectrum of $\{\mathbf{9}\}_2$ recorded at −80 °C shows likewise two signals which coalesce, however, to a single line at higher temperature. The ^1H and ^{13}C NMR spectra display also intricate temperature dependent coalescence phenomena. In addition, a new, extremely broad resonance ($\Delta\nu_{1/2}$ = 7100 Hz at r.t., *cf.* Fig. S3 in the ESI†) grows in when the temperature is raised and reversibly disappears upon cooling. We attribute this signal to radical **9**, the presence of which was independently proven by EPR spectroscopy (see below). Altogether, the observed spectral changes indicate the simultaneous occurrence of two dynamic processes, *viz.* reversible equilibration between $\{\mathbf{9}\}_2$ and two radicals **9** (which enables also interconversion between *rac*- and *meso*-$\{\mathbf{9}\}_2$), and freezing of the TMP ring inversion at low temperature. It should be noted that there is ample literature precedence

¶Even if the electron density of the phosphorus lone-pairs is not visible in the crystal structure, the conformation of $\{\mathbf{9}\}_2$ suggests an ecliptic orientation of the lone-pairs and the P1–N12/P1′–N12′ bonds.

Table 2 EPR parameters of persistent aminophosphanyl radicals **3c**, **4–9**

	g	a(^{31}P) [G]	a(^{14}N)[a] [G]	Further splittings[a]	Ref.
3c	2.0248	42	5.4 (2 N)	—	4*g*
4	2.0031	60.9	3.7 (2 N)	a(^{1}H) = 2.9 G (4 H)	4*j*
5	2.014	63.8	4.3 (2 N)	a(^{1}H) = 3.8 G (2 H)	4*l*
6	2.0055	75.5	3.8 (2 N)	—	This work
7	2.0047	76.2	5.6 (1 N)	a(^{29}Si) = 12.2 G	This work[b]
8	2.0045	83.5	5.8 (1 N)	a(^{1}H) = 2.6 G (4 H)	This work
9	2.0047	84.7	5.7 (1 N)	a(^{1}H) = 1.2 G (2 H)	This work

[a] Number of interacting nuclear spins given in parentheses. [b] Published data from ref. 4*a* and *c*: g = 2.0046–2.007, a(^{31}P) = 75.9–77.2 G, a(^{14}N) = 5.2–5.95 G.

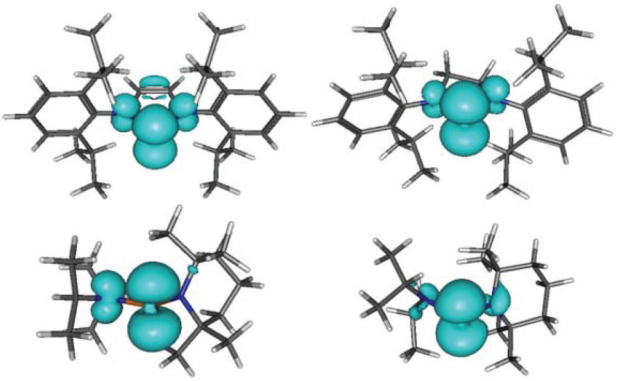

Fig. 3 Representation of computed (ωB97x-D/cc-pVDZ) spin densities in the radicals **3c** (top left), **4** (top right), **9** (bottom left), and a second conformer of **9** with skewed alignment of R_2N-groups (bottom right; skew angles 69° and 59°). The two conformers of **9** illustrate the dependence of N-centred spin density on skew angles. The drawn isodensity surfaces include 75% of the total spin density.

for the spectroscopic observation of equilibration between persistent phosphanyl radicals and their dimers,[4c,e,j–l] but $\{\mathbf{9}\}_2$ is to the best of our knowledge the first example where the coexistence of both reactants has been established by NMR spectroscopy.

Direct characterization of radicals was feasible by recording EPR spectra of solutions of $\{\mathbf{4}\}_2$–$\{\mathbf{9}\}_2$ in inert solvents (hexane, toluene). The signals of the radicals were readily observed at ambient (**4**, **9**) or elevated temperature (**5–8**) and analysed by simulation using the EasySpin[12] program (Table 2).

The spectral parameters of **4**, **5** and **7** match previously published data.[4a,c,j,l] All signals are split into multiplets due to hyperfine coupling with the nuclear spins of the ^{31}P (I = 1/2) and one (**7–9**) or two (**4–6**) ^{14}N (I = 1) nuclei. In some cases, additional couplings to remote ^{1}H or ^{29}Si nuclei are resolved. The hyperfine couplings to phosphorus (60–84 G) are larger than in **3c** (a(^{31}P) = 42 G [4k]) and cover roughly the lower half of the range of couplings (63–108 G [2a]) in known phosphanyl radicals. The absence of resolved hyperfine coupling to one ^{14}N nucleus in **7** had been previously noted and was attributed to the fact that couplings to nitrogen atoms in silylamino-groups are usually unobservable,[4a,c] presumably since their steric bulk prevents a coplanar orientation of the phosphorus and nitrogen coordination planes.[2a] The spectra of **8**, **9** reveal, however, that unequal a(^{14}N) couplings are also observable in dialkylamino-substituted phosphanyl radicals and the absence of resolved coupling to ^{14}N is thus not specific for silylamino groups.

Computational studies on different conformers of **6–9** confirm the expectation[2a,4a] that the spin density resides mainly in the phosphorus p-orbital and reveal further that its delocalization on the nitrogen atoms shows a marked conformational dependence that is largely independent of substituent type (Fig. 3 and Table 3): maximum values of the spin density, and hence the hyperfine coupling constant (a(^{14}N) 5–6 G), are found when the coordination planes at the phosphorus and nitrogen atoms are coplanar, and minimum values (|a(^{14}N)| < 1 G) when they are close to perpendicular.

Based on this correlation, we can confirm the association of the large hyperfine coupling in **7** with the $NiPr_2$ group[4a,c] and

Table 3 Calculated hyperfine splittings and skew angles for **4–9** at the ωB97x-D level

		a(^{31}P)[a] [G]	a(^{14}N)[a,b] [G]	Skew angle[a] [°]
3c		56.4 (59)	6.6 (18)[c]	5[c]
4		75.9 (76)	5.8 (11)	8
			3.9 (11)	9
5		74.6 (76)	5.7 (11)	5
			5.5 (10)	8
6		77.2 (76)	5.1 (10)[c]	44[c]
7	$NiPr_2$	81.1 (77)	5.9 (18)	21
	$N(SiMe_3)_2$		0.4 (1)	73
8	NEt_2	96.5 (80)	5.9 (14)	16
	TMP		−0.8 (1)	82
9	$NiPr_2$	87.7 (86)	6.1 (6)	15
	TMP		−1.1 (2)	82

[a] Numbers in parentheses denote the percentage of NPA spin density on the appropriate atom. [b] A plot of a(^{14}N) *vs.* skew angle is shown in Fig. S2 in the ESI. [c] Two identical NR_2 moieties.

conclude further that the splittings in the spectra of **8**,**9** arise from interaction with the NR_2 (R = Et, iPr) groups and the coupling to the TMP substituent is unresolved. The observation that a(^{14}N) in **4–6** is smaller than in **7–9** (Table 2) may be attributable to the presence of librational motion of the R_2N-groups in the real molecules which cannot be reproduced computationally. However, the calculations support the earlier conjecture[4g] that the reduction of a(^{31}P) and simultaneous increase of a(^{14}N) in **3c** coincides with extended delocalization of the spin density over the complete ring (Fig. 3).

Thermochemistry of diphosphane dissociation

Thermochemical parameters for the dissociation of the diphosphanes according to R_2P–$PR_2 \rightleftarrows 2\ R_2P^{\bullet}$ may be derived from the temperature dependent variation of the equilibrium con-

Table 4 Experimental thermochemical data (free energy ΔG^{295}_{Diss} and equilibrium constant K^{295} at 295 K, reaction enthalpy ΔH_{Diss} and entropy ΔS_{Diss}) for the dissociation reaction $R_2P–PR_2 \rightleftarrows 2\ R_2P^{\bullet}$ (R_2P = **3c**, **4–9**). Numbers in parentheses denote estimated standard deviations

Diphosphane	ΔG^{295}_{Diss} [kJ mol^{-1}]	pK^{295}_{Diss} [a]	ΔH_{Diss} [kJ mol^{-1}]	ΔS_{Diss} [J (mol K)$^{-1}$]
{**3c**}$_2$ [b]	26.8(8)	4.8(8)	78.8(8)	176(15)
{**4**}$_2$	69.4(21)	12.3(22)	102.3(11)	112(4)
{**5**}$_2$	88.6(17)	15.7(28)	104.9(10)	55(3)
{**6**}$_2$	70.2(21)	12.4(4)	108.9(12)	131(4)
{**7**}$_2$	69.6(28)	12.3(5)	95.4(14)	87(5)
{**8**}$_2$	66.9(23)	11.9(4)	99.5(12)	110(4)
{**9**}$_2$	13(7)	2.3(12)	64.2(30)	174(13)

[a] $pK^{295}_{Diss} = -\lg(K_{Diss}(295\ K)/[mol\ l^{-1}])$. [b] Data from ref. 4*k*.

stant $K = c(R_2P^{\bullet})^2/c(R_2P–PR_2)$. The latter can be determined by measuring the radical concentration in a sample prepared by dissolution of a known amount of solid diphosphane, and then back-calculating the actual concentration of the diphosphane in solution. The radical concentration is readily obtained from the double integral of the EPR signal in relation to that of a reference sample with a known number of spins.[12] Following this approach, we determined the concentration of radicals **4–9** in solutions of {**4**}$_2$–{**9**}$_2$ against a calibrated sample of ultramarine blue by using a previously published procedure.[4k] A summary of the thermochemical parameters derived from these measurements is given in Table 4, and a detailed account is contained in the ESI.†

Evaluation of the data in Table 4 reveals that although the radicals **4–9** are spectroscopically readily observable as persistent species at ambient or elevated temperature, the dissociation equilibria lie in all cases but {**9**}$_2$ extensively on the side of the diphosphanes, and the dissociation affects generally far less than 1% of the dimers even at temperatures as high as 120 °C. In case of {**9**}$_2$, the calculated degree of dissociation for a solution of 1 mM initial concentration of 0.65(5) at 295 K clearly exceeds the value of 0.063(7) for **3c**, and attests that radicals predominate under these conditions.

The observation of a large variability in ΔH_{Diss} and ΔS_{Diss} reveals, however, that structural changes have nonetheless a significant impact on the energetics of the bond fission. Comparing the dissociation energetics of {**4**}$_2$ and {**5**}$_2$ with that of {**3c**}$_2$ shows that introduction of the CC double bond goes along with a decrease in ΔH_{Diss} by some 23–25 kJ mol^{-1}. In view of the presence of identical or at least similar substituents in all species, attractive dispersion forces between the two R_2P fragments in the dimers are not expected to change greatly, and the lower dissociation enthalpy for {**3c**}$_2$ is thus considered to reflect mainly the postulated[4g] extra stabilization of radical **3c** by π-delocalization effects.

It should be noted, however, that the exceptional dissociation tendency of {**3c**}$_2$ (as evidenced by the drastic decrease of ΔG^{295}_{Diss} as compared to {**4**}$_2$ and {**5**}$_2$) is not attributable to the enthalpy lowering alone, but is assisted by a simultaneous large increase in the entropic term. Since the translational contribution to the reaction entropy is identical in all cases, this change implies that the loss of internal conformational flexibility associated with radical dimerization must increase significantly from **5** over **4** to **3c**. Without going into detail, we presume that the difference between the last two species owes to the rigidity of the unsaturated heterocyclic ring in **3c**, which severely reduces the conformational freedom of the *N*-aryl groups. The further shift of the dissociation equilibrium to the side of the dimer in case of {**5**}$_2$ is exclusively attributable to the change in ΔS_{Diss} and may be qualitatively explained by assuming that the restrictions in the conformational freedom upon dimerization decrease with the number of bulky *o*-alkyl substituents in the *N*-aryl moieties.

Aggravating conformational restrictions with increasing steric demand of substituents may also help to rationalize the observation that the values of ΔS_{Diss} in the acyclic diphosphanes {**7**}$_2$–{**9**}$_2$ exhibit comparable changes as in the heterocycles **3c–5**. Apart from that, the dissociation enthalpies are for {**7**}$_2$, {**8**}$_2$ by some 5–10 kJ mol^{-1} lower than for {**4**}$_2$, {**5**}$_2$, and display a further sharp decrease in case of {**9**}$_2$ where ΔH_{Diss} is even smaller than for {**3c**}$_2$. While this last finding is deemed to reflect the exceptional degree of strain that had already become evident in the extreme P–P bond lengthening and enforcement of the energetically unfavourable *pseudo*-ecliptic conformation, the reason for the low dissociation enthalpies in {**7**}$_2$ and {**8**}$_2$ is at first glance less obvious. We assume, however, that their increased conformational flexibility enables the acyclic $(R_2N)_2P$ moieties to yield to the steric congestion upon dimerization as in the case of {**1P**}$_2$ [6] and {**7**}$_2$ [4d] by a distortion of dihedral angles that loads the dimers with some extra steric strain energy. Since the release of this energy during dissociation in a "Jack-in-the-box" manner[6] amounts to a relative stabilization of the radicals, this effect is suitable to explain the reduction of ΔH_{Diss} in comparison to the cyclic derivatives where the conformational constraints of the ring render such structural relaxation unfeasible.

Last, but not least, {**6**}$_2$ shows the largest value of ΔH_{Diss} of all derivatives in this study which is, however, compensated by an unusually high entropic contribution that must be seen as main driving force of the dissociation. Whereas the large dissociation enthalpy is not unexpected if one considers that the moderately sized *N*-alkyl groups seem inappropriate for loading the dimer with a large amount of strain energy, we have currently no good explanation for the atypically large entropy term.

Computational studies

In order to validate our hypotheses on the origin of the trends in dissociation enthalpies and improve our understanding of the bond fission process, we performed computational studies of the dissociation reactions of {**4**}$_2$–{**9**}$_2$. Acknowledging that a realistic description of molecular structures and energetics requires inclusion of long-range and dispersion interactions,[4k,8] all calculations were carried out at the ωB97x-D/cc-pVDZ level which had been previously shown to give an appropriate description of the molecular structure of {**3c**}$_2$.[4k] Mole-

Table 5 Bond distances (P–P in Å) and energy data (all quantities in kJ mol^{-1}) for the dissociation reaction $R_2P–PR_2 \rightleftarrows 2R_2P^{\bullet}$ (R_2P = **3c**, **4**–**9**) computed at the ωB97x-D/cc-pVDZ level of theory

	P–P	ΔE_{zpe}	ΔE_{relax}	ΔE_{frag}	$E^{D\,a}$	ΔH^{298}	ΔG^{298}
{**3c**}$_2$	3.323[b]	120.5[b]	59.5	196.4	153.3	129.9[b]	5.9[b]
{**4**}$_2$	2.317	155.3	41.2	208.9	147.1	158.4	66.4
{**5**}$_2$	2.301	156.8	51.4	219.2	100.9	157.4	79.7
{**6**}$_2$	2.296	119.0	79.9	214.8	79.8	123.3	39.0
{**7**}$_2$	2.278	98.6	106.4	234.8	102.2	105.6	9.5
{**8**}$_2$	2.296	85.5	121.7	223.2	75.8	19.9	0.4
{**9**}$_2$	2.348	51.5	121.3	193.8	97.3	10.3	−9.4

[a] E^D = contribution from empirical dispersion terms. [b] Data from ref. 4*k*.

cular geometries of dimers and radicals were first energy optimized using the solid-state structures as starting points, and the nature of the final geometries as local minima on the energy hypersurface was then validated by frequency calculations. In case of the radicals **7**–**9** and the diphosphanes {**4**}$_2$, {**6**}$_2$, and {**8**}$_2$, we located alternative conformers that were likewise local minima on the energy hypersurface but proved energetically less stable (ΔE 19.5 kJ mol^{-1} for *trans*-{**4**}$_2$ *vs.* *gauche*-{**4**}$_2$, 65.9 kJ mol^{-1} for *trans*-{**6**}$_2$ *vs.* *gauche*-{**6**}$_2$, and 13.2 kJ mol^{-1} for *gauche*-{**8**}$_2$ *vs.* *trans*-{**4**}$_2$) and were not considered further. Computed and experimental geometries of the dimers are generally in good agreement, with the single exception that the P–P distance in {**4**}$_2$ is significantly overestimated. Comparison of calculated (Table 5) and experimental (Table 1) P–P distances for the remaining compounds yields a liner relation $P–P_{calc}$ = 0.95 $P–P_{exp}$ + 0.11 Å (R^2 = 0.93). The computations reproduce also the molecular conformation of **7** determined by gas phase electron diffraction.[4d] Comparing the geometries of the $(R_2N)_2P$ units in radicals and diphosphanes reveals that formation of N-heterocyclic radicals is mainly associated with a deformation of bond angles at the nitrogen atoms, whereas formation of acyclic species involves also appreciable conformational changes (see Fig. S12†).

Energies (including corrections for zero point vibrational energy, ΔE_{zpe}) and (free) enthalpies (ΔH^{298}, ΔG^{298}) for the dissociation reactions were computed with the inclusion of basis set superposition errors as determined from counterpoise calculations and are listed in Table 5. In addition, we computed also a decomposition[13] of the total reaction energy into a fragmentation energy ΔE_{frag} (the negative of the interaction energy[13] E_{int} between two radical fragments having the same geometry as the R_2P units in the dimer) and a relaxation energy ΔE_{relax} (the energy released upon relaxation of the distorted radicals to their equilibrium geometry, *i.e.* the negative of the preparation energy[13] ΔE_{prep}).

Comparison of absolute values and trends in computed (ΔH^{298}) and experimental (ΔH_{Diss}) dissociation enthalpies (Fig. 4) reveals a reasonable match for *N*-alkyl-/silyl-substituted diphosphanes ({**6**}$_2$–{**9**}$_2$) while the dissociation enthalpies of *N*-aryl derivatives ({**3c**}$_2$–{**5**}$_2$) are clearly overestimated in the

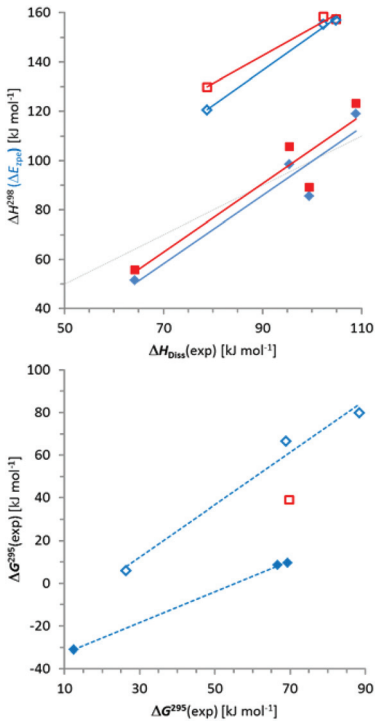

Fig. 4 Top: Plot of calculated energies (ΔE_{zpe} including zero-point vibrational correction, red squares) and enthalpies of dissociation (ΔH^{298}, blue diamonds) *vs.* experimental values of ΔH_{Diss}; bottom: Plot of calculated free energies of dissociation (ΔG^{298}) *vs.* experimental values of ΔG^{295}. Open and filled symbols refer to *N*-aryl ({**3c**}$_2$–{**5**}$_2$) and *N*-alkyl/silyl derivatives ({**6**}$_2$–{**9**}$_2$), respectively. Red and blue trend lines were determined from linear regression analysis (the red square in the lower plot refers to {**6**}$_2$ and is considered an outlier), and the dotted grey line denotes the relation ΔH^{298} = ΔH_{Diss}.

computations (as had already been noted for **3c**[4k]).‖ A similar result emerges for comparison of ΔE_{zpe} with ΔH_{Diss} (Fig. 4). While it is known that most density functionals have problems with a proper description of the difference in intermolecular binding energies between aromatic and aliphatic moieties,[14] a deviation of some 50 kJ mol^{-1} as found here is far too large to refer to this explanation, and we are currently unable to provide a consistent rationalization for this effect.

Computed free enthalpies ΔG^{298} (Table 5) are generally much smaller than the experimental values (Table 4), which is mainly due to the fact that the computations heavily overestimate the entropy terms. This deviation may in part reflect the difference between gas phase and solution (it has been claimed that the entropy contribution to ΔG in solution at room temperature is roughly half of that in the gas phase[15]) and had been noted previously.[4k] With the exception of {**6**}$_2$, which we consider an outlier, a comparison between computed and experimental free enthalpies gives a similar result as had already been observed for the enthalpies (Fig. 4).

‖ A similar deviation between calculated bond enthalpies/energies of *N*-alkyl/silyl- and *N*-aryl-substituted diphosphanes was also found at the M06-2X/cc-pVDZ level.

The results of the energy decomposition analysis listed in Table 5 indicate that the variations in ΔE_{frag} are not only much smaller than those of the total energy term (ΔE_{zpe} or ΔH^{298}), but show also a different response to structural changes. With the exception of $\{\mathbf{3c}\}_2$ (where a contribution from electronic stabilization by π-delocalization must be taken into account), ΔE_{frag} in both N-heterocyclic and acylic compounds dwindles with increasing steric demand of the substituents, which suggests that its variation reflects mainly the bond weakening or strengthening associated with the modulation of repulsive interactions between bulky peripheral groups. Given that the P–P bond lengthening in sterically congested diphosphanes is commonly ascribed to the same origin,[8] it is not surprising that the changes in ΔE_{frag} – unlike those in the total energy terms (ΔE_{zpe} or ΔH^{298}) or experimentally determined enthalpies ΔH_{Diss} – correlate with the variation in P–P distances (Fig. 5). Even if a clear-cut partitioning between 'intrinsic' bond energy and strain energy in congested molecules is not a trivial task,[7] we conclude that ΔE_{frag} can serve as an – at least approximate – measure of P–P bond strength. Since the values of ΔE_{frag} come close to the average P–P bond enthalpy[9] of 201 kJ mol^{-1} and approach the dissociation energies of sterically uncongested diphosphanes (239–368 kJ mol^{-1} for R_2P–PR_2 with R = H, Et, F, Cl, I[16]), the P–P bonds in $\{\mathbf{3c}\}_2$–$\{\mathbf{9}\}_2$ cannot be considered as intrinsically particularly weak. It must be conceded, however, that as in case of **1**[8] attractive dispersion forces (epitomized by the empirical dispersion term E^D) make a considerable contribution to the total adhesion energy. This contribution is clearly dominant for $\{\mathbf{3c}\}_2$ and $\{\mathbf{4}\}_2$ where it represents 70–80% of the fragmentation energy.

The relaxation energies ΔE_{relax} which stabilize the radicals **3c–9** through structural adaptation and conformation changes are, like in **1P**,[8] smaller than the fragmentation energies, but with 20–60% of the magnitude of ΔE_{frag} still substantial. Furthermore, the variation between different radicals ($\Delta\Delta E_{relax}$ = 80.5 kJ mol^{-1}) is twice as large as that of the fragmentation energies ($\Delta\Delta E_{frag}$ = 41.0 kJ mol^{-1}) and must thus be seen as the dominant energetic contribution in explaining the trend in dissociation energies between different diphosphanes. Structural relaxation of the acyclic radicals **6–9** provides generally a larger energy release (ΔE_{relax} 80–122 kJ mol^{-1}) than relaxation of the N-heterocyclic species **3c–5** (ΔE_{relax} 41–60 kJ mol^{-1}) and is associated with additional conformational changes (Fig. S12 in the ESI†). These findings support at first glance the perception of the dimers $\{\mathbf{6}\}_2$–$\{\mathbf{9}\}_2$ as sterically strained "Jack-in-the-box" molecules which can release their strain energy by undergoing geometrical *and* conformational adaptation during dissociation. However, we must also consider that the variation in skew angles or the pyramidalization of NR_2 groups associated with a conformational change may affect the spin density delocalization, and thus the electronic stability, of the radicals. In order to assess the importance of these effects, we analysed the conformational preferences of the parent diaminophosphanyl radical $(H_2N)_2P^\bullet$ ($\mathbf{10}^\bullet$) and the appropriate cation $[(H_2N)_2P^+]$ ($\mathbf{10}^+$), assuming that the impact of steric constraints is in these species negligible and any changes will be dominated by electronic effects. Geometry optimizations were carried out using DFT (B3LYP with (aug)-cc-pVDZ and aug-cc-pVTZ basis sets) and coupled cluster (CCSD/aug-cc-pvdz) methods. The results did not differ significantly, and we will only discuss those of the CCSD calculations (Fig. 6).

The cation $\mathbf{10}^+$ exhibits, as expected, a C_{2v}-symmetrical planar geometry with rather short PN distances of 1.643 Å. Geometry optimization of a conformer obtained by rotation of one NH_2 group by 90° led to the localization of a transition state 17.8 kJ mol^{-1} higher in energy than the ground state. The 'orthogonal' amino substituent is characterized by a lengthened PN bond (1.715 *vs.* 1.632 Å for the 'in plane' NH_2 group) and a slightly pyramidal geometry at the N-atom. The computational results are in accord with the established view of aminophosphenium ions[17,18] as delocalized, allyl-anion analogue π-systems in which rotation of NR_2 groups (which partially disrupts the π-delocalization) is impeded by a significant energy barrier. In contrast, radical $\mathbf{10}^\bullet$ features a non-planar, C_2-symmetrical ground state geometry with twisted orientation of the NH_2 groups (skew angle 30°), pyramidal coordination at the N-atoms (sum of bond angles 343°) and lengthened PN bonds (1.752 Å). The search for a rotational transition state yielded a C_1-symmetrical geometry in which the average PN distance remains essentially unchanged (PN 1.773, 1.737 Å,

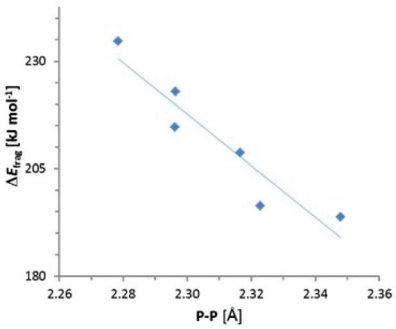

Fig. 5 Plot of computed fragmentation energies ΔE_{frag} *vs.* bond distances. The straight line is the result of a linear regression analysis (R^2 = 0.89).

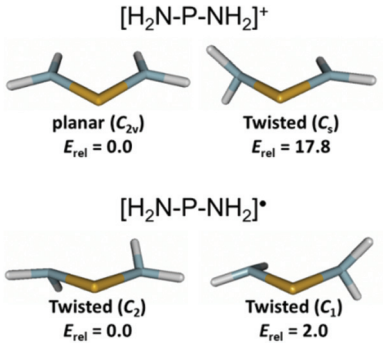

Fig. 6 Computed molecular structures and relative energies (in kJ mol^{-1}) at the CCSD/aug-cc-pVDZ level of theory for the electronic ground states (left) and rotational transition states (right) of $\mathbf{10}^+$ and $\mathbf{10}^\bullet$.

average 1.755 Å) and the pyramidalization in the 'orthogonal' NH_2 group increases further (sum of bond angles at N 331°). The transition state energy lies by merely 2.0 kJ mol^{-1} above that of the ground state, indicating that the energetic barrier to NH_2-group rotation is negligible and the geometrical changes associated with this process do not affect radical stability. This pronounced difference to the cation is easily rationalized if one considers that placement of an extra electron in the (PN-antibonding) LUMO of the cation reduces the π-bond order, and thus the available stabilization from π-delocalization. Consequently, the remaining interaction between an unpaired electron on the P-atom and the nitrogen lone-pairs in aminophosphanyl radicals should be better described as hyperconjugative, and its tuning by rotational reorientation of NH_2 (or NR_2) groups offers – unlike as in aminophosphenium ions[17] – only minor opportunities for electronic (de) stabilization.

The computational studies on $\mathbf{10}^+$ and $\mathbf{10}^\bullet$ imply that the orientational preorganisation of phosphorus p-orbitals and nitrogen lone-pairs which arises from embedding of an NPN into a five-membered heterocycle[18,19] offers an energetic advantage for aminophosphenium cations, but not for radicals, and that the NPN unit of the latter provides, apart from possible constraints imposed by a cyclic molecular structure, no further restoring force to maintain local planarity. We are thus prompted to conclude that the structural reorganization of the radicals formed during dissociation of tetraaminodiphosphanes is not associated with any extra electronic stabilization of the unpaired electron, but is essentially driven by steric factors. In turn, the inhibition of structural relaxation by a geometrical constraining cyclic structure must be considered to have an adverse effect on dissociation enthalpies, which helps to explain why P–P bond fission is slightly more endothermic for the heterocyclic dimers $\{\mathbf{3c}\}_2$–$\{\mathbf{5}\}_2$ than for $\{\mathbf{7}\}_2$–$\{\mathbf{9}\}_2$.

Conclusions

Thermochemical data for the homolytic P–P bond fission of a series of sterically congested diphosphanes (two of which were newly synthesized and fully characterized) were determined. The values of free reaction energies ΔG^{295}_{Diss} and pK^{295}_{Diss} indicate that the dissociation affects in most cases only a small fraction of the diphosphanes, and the concentration of persistent radicals – even if they may be spectroscopically observable at ambient temperature – remains small. A notable exemption is $\{\mathbf{9}\}_2$ where the degree of dissociation (for a 1 mM solution at 295 K) is by an order of magnitude larger than for the N-heterocyclic diphosphane $\{\mathbf{3c}\}_2$. The acyclic radical **9** must thus be considered as even more stable than **3c** which benefits from electronic stabilization by π-delocalization.[4g]

Analysis of trends in experimental data in connection with computational studies allowed us to relate the variations in $\Delta G^{295}_{Diss}/pK^{295}_{Diss}$ to both enthalpy and entropy effects. Stabilization of radicals relative to dimers with a concomitant decrease in dissociation enthalpies ΔH_{Diss} is mainly due to structural relaxation (adaptation of bond angles and – for the acyclic species **6–9** – conformational changes) and driven by the need to minimize steric congestion. Electronic stabilization by P,N-π-conjugation, which is crucial for aminophosphenium cations,[17,18] is hardly of importance for aminophosphanyl radicals, and the energetic effect of cyclic π-delocalization in **3c** is visible but stands back. The radical stabilizing influences are offset by strong attractive dispersion forces, which are once more[8] confirmed as crucial for the prevalence of diphosphanes. Entropic factors driving the dissociation can be qualitatively related to the gain of conformational flexibility in the radicals, although their origin is not yet understood in detail and cannot be adequately modelled computationally. Still, the supplement of the enthalpic stabilization of the radicals by a particularly large entropic contribution must be seen as decisive for the extensive dissociation of $\{\mathbf{9}\}_2$ (and $\{\mathbf{3c}\}_2$).

It should be noted that our results are in principle in accord with the results of a computational study on the dimerization of the radicals **1**[8] stating that the monomer – dimer equilibrium is predominantly governed by the balance of attractive dispersion forces and entropic factors. However, the results presented here emphasize that the different aspects of structural relaxation (in particular the conformational changes enabling "Jack-in-the-box" behaviour[6]) are also vital for the explanation of the trends in dissociation enthalpies and entropies between different molecules. Furthermore, it appears that computational models tend to overestimate the entropy term associated with the diphosphane dissociation, and yield thus free reaction energies which are systematically too low.

Experimental

Materials and methods

All manipulations were carried out under dry argon. Solvents were dried by standard procedures. NMR spectra were recorded on Bruker Avance AV 400 or AV 250 instruments (^{1}H: 400.1/250.0 MHz, ^{13}C: 100.5/62.9 MHz, ^{31}P: 161.9/101.2 MHz); chemical shifts were referenced to ext. TMS (^{1}H, ^{13}C), 85% H_3PO_4 (Ξ = 40.480747 MHz, ^{31}P). Elemental analyses were carried out using an Elementar Micro Cube. Melting Points were determined with a Büchi B-545 melting point apparatus in sealed capillaries. EPR spectra were measured with a Bruker EMX X-band spectrometer. Hyperfine splittings were determined by spectral simulation with the program EasySpin.[12] Quantitative EPR measurements and evaluation of thermochemical data from the spectral data were carried out using the same protocol that had been applied in case of $\{\mathbf{3c}\}_2$. A detailed description has been given elsewhere.[4k]

Chlorophosphane precursors (iPr_2NPCl_2,[19] $(Me_3Si)_2N(iPr_2N)PCl$,[4a] $(iPr_2N)_2PCl$,[20] and (TMP)(iPr_2N)PCl[21]) and the diphosphanes $\{\mathbf{4}\}_2$,[4j] $\{\mathbf{5}\}_2$ [4l] and $\{\mathbf{6}\}_2$,[10] were prepared as described elsewhere. Diphosphane $\{\mathbf{7}\}_2$ was prepared by a modification

of the reported procdure,[4c] using sodium naphthalenide instead of potassium graphite as reducing agent.

Synthetic procedures

Chloro(diethylamino)(2,2,6,6-tetramethylpiperidyl)phosphane 8_Cl. *n*BuLi (4.5 mL of a 2.3 M solution in hexane, 10.50 mmol) was added dropwise at −78 °C to a solution of 2,2,6,6-tetramethylpiperidine (1.80 mL, 10.50 mmol) in THF (10 mL). The mixture was then allowed to warm to room temperature and stirred for 30 min. This solution was then added dropwise to a cooled (−78 °C) solution of Et_2NPCl_2 (1.83 g, 10.50 mmol) in THF (15 mL). The reaction mixture was allowed to warm to room temperature and stirred overnight. Volatiles were then removed under reduced pressure. The residue was extracted with 15 mL hexane and filtered. The filtrate was evaporated to dryness under reduced pressure and the resulting orange oil used without further purification. Yield 2.46 g (84%). – $^{31}P\{^1H\}$ NMR ($CDCl_3$): δ = 170.5. ^1H NMR ($CDCl_3$): δ = 3.06 (dq, $^2J_{PH}$ = 10.0 Hz, $^3J_{HH}$ = 7.0, 4 H, CH_2), 1.65–1.35 (m, 18 H, TMP), 1.02 (t, $^3J_{HH}$ = 7.0 Hz, 9 H, CH_3). $^{13}C\{^1H\}$ NMR ($CDCl_3$): δ = 57.0 (d, $^2J_{PC}$ = 12.5 Hz, N*C*), 40.9 (d, $^2J_{PC}$ = 0.7 Hz, NCH_2), 39.1 (d, $^3J_{PC}$ = 17.5 Hz, $NCCH_2$), 30.7 (br s, CH_3), 16.1 (d, $^4J_{PC}$ = 1.0 Hz, $NCCCH_2$), 12.7 (d, $^3J_{PC}$ = 3.0 Hz, CH_3).

1,2-Bis(Diethylamino)-1,2-bis(2,2,6,6-tetramethylpiperidyl)-diphosphane {8}$_2$. Mg chips (excess) and a crystal of I_2 were added to a solution of **8_Cl** (1.21 g, 4.1 mmol) in THF (10 mL). The mixture was heated for 3 h to 48 °C in an ultrasound bath. The solvent was then removed under reduced pressure and the residue extracted with 10 mL of hexane and filtered. The filtrate was stored at −24 °C until a crystalline product formed. Yield 0.50 g (25%). – M.p. 98 °C. – $^{31}P\{^1H\}$ NMR (C_6D_6): δ = 99.2, 91.6 (s). Isomer A: ^1H NMR (C_6D_6): δ = 3.35 (m, 8 H, CH_2CH_3), 1.72–1.67 (m, 12 H, $CH_2CH_2CH_2$), 1.40 (br s, 24 H, CH_3), 1.11 (t, 12 H, $^3J_{HH}$ = 7.2 Hz, CH_2CH_3). Isomer B: ^1H NMR (C_6D_6): δ = 3.40 (m, 8 H, CH_2 CH_3), 1.67–1.63 (m, 12 H, $CH_2CH_2CH_2$), 1.52 (s, 12 H, CH_3), 1.49 (s, 12 H, CH_3), 1.13 (t, 12 H, $^3J_{HH}$ = 7.3 Hz, CH_2CH_3). – $^{13}C\{^1H\}$ NMR (C_6D_6): δ = 45.5 (br s, NCH_2), 38.4–27.5 (br m, $(CH_2)_3$), 31.6 (br s, CH_3), 13.8 (br s, CH_2CH_3). Quaternary carbon atoms could not be detected because of the low signal-to-noise ratio. –$C_{26}H_{56}N_4P_2$, (M = 486.69 g mol^{-1}): calcd C 64.16 H 11.60 N 11.51; found C 63.49 H 11.56 N 11.31.

1,2-Bis(diisopropylamino)-1,2-bis(2,2,6,6-tetramethylpiperidyl)-diphosphane {9}$_2$. Blank pieces of sodium (excess) were added to a solution of TMP(iPr_2N)PCl (1.51 g, 4.9 mmol) in 10 mL of hexane which had previously been degassed using the pump-and-freeze technique. The mixture was then heated for 7 h at 48 °C in an ultrasound bath, allowed to cool to ambient temperature, and filtered. The filtrate was evaporated to dryness and the residue sublimated in vacuum (10^{-3} mbar, 90 °C) to give the product as colourless solid. Yield 33%. – M.p. 86 °C. – $^{31}P\{^1H\}$ NMR (C_6D_6): δ = 106.4 (s). ^1H NMR (C_6D_6): δ = 4.61 (br m, 2 H, $CHCH_3$), 3.31 (br m, 2 H, $CHCH_3$), 1.81 (br, 12 H, $C(CH_3)_2$), 1.81 (br, 2 H, CH_2), 1.81 (br, 2 H, CH_2), 1.69 (br, 2 H, CH_2), 1.63 (br, 12 H, CH_3), 1.57 (br, 6 H, $CHCH_3$), 1.52 (br, 6 H, $CHCH_3$), 1.47 (br, 2 H, CH_2), 1.46 (br, 6 H, $CHCH_3$), 1.43 (br, 2 H, CH_2), 1.38 (br, 6 H, $CHCH_3$), 1.29 (br, 2 H, CH_2). – $^{13}C\{^1H\}$ NMR (C_6D_6): δ = 42.7 (br, CH_2), 42.4 (br, CH_2), 34.7 (br, CH_3), 30.5 (br, CH_3), 29.9 (br, CH_3), 26.9 (br, $CHCH_3$), 26.6 (br, $CHCH_3$), 23.8 (br, $CHCH_3$), 22.4 (br, $CHCH_3$), 18.9 (br, CH_2); the remaining ternary and quaternary carbon atoms could not be detected because of the low signal to noise ratio. – $C_{30}H_{64}N_4P_2$ (542.82 g mol^{-1}): calcd C 66.38 H 11.88 N 10.32; found C 65.86, H 11.87, N 10.08.

Crystal structure determinations

Diffraction studies were carried out using a Bruker diffractometer equipped with an Kappa APEX II Duo CCD-detector and a KRYO-FLEX cooling device with Mo-K_α radiation (λ = 0.71073 Å) at T = 100 K. The structures were solved by direct methods (SHELXS-97[22a]) and refined with a full-matrix least-squares scheme on F^2 (SHELXL-2014[22b]). Semi-empirical absorption corrections were applied for all structures. Non-hydrogen atoms were refined anisotropically, and H atoms with a riding model, on F^2. Details of the crystal structure determinations are listed in Table 6. For {**9**}$_2$, the absolute structure parameter[22c] was refined as x = 0.00(10). Details of the crystal structure determinations are listed in Table 6 (for **9_Cl** in the ESI†).

Table 6 Crystallographic data for {**8**}$_2$ and {**9**}$_2$

	{**8**}$_2$	{**9**}$_2$
CCDC	1414815	1414816
Formula	$C_{26}H_{56}N_4P_2$	$C_{30}H_{64}N_4P_2$
Formula weight	486.69	542.79
Crystal size (mm)	0.21 × 0.08 × 0.07	0.12 × 0.11 × 0.10
T [K]	100(2)	100(2)
Crystal system	Monoclinic	Orthorhombic
Space group	$P2_1/n$	$P2_12_12$
a (Å)	8.3594(6)	16.522(2)
b (Å)	9.0786(6)	17.526(2)
c (Å)	18.6456(12)	11.2185(15)
β (°)	β = 92.968(3)	90
V (Å^3)	1413.15(17)	3248.5(7)
Density (Mg m^{-3})	1.144	1.110
F(000)	540	1208
Z	2	4
Abs. coeff. μ (mm^{-1})	0.174	0.158
Absorption correction	Semiempirical from equivalents	Numerical
Data collected	19 704	20 756
Unique data	2901	5756
Observed data with $I > 2\sigma(I)$	2248	3419
Restraints	0	0
Variables	145	325
R_1 ($I > 2\sigma(I)$)	0.041	0.066
wR_2	0.108	0.113
GOF	1.034	0.992
Max. diff. dens. (e Å^{-3})	0.483	0.329
Min. diff. dens. (e Å^{-3})	−0.302	−0.313

Computational studies

Computational studies were performed with the Gaussian09[23] suite of programs. Computations on **4–9** and $\{\mathbf{4}\}_2$–$\{\mathbf{9}\}_2$ were carried out using the ωB97X-D functional by Head-Gordon[24] with cc-pVDZ basis sets. Explorative calculations were also carried out with Truhlar's M06-2X functional[25] and the same basis. Attempts to use larger basis sets (*i.e.* including diffuse funtions or of triple zeta quality) failed due to numerical or computation time problems. Numerical integrations were performed on an ultrafine grid. Since an attempt to model the dissociation of $\{\mathbf{6}\}_2$ in solution showed that inclusion of solvent effects by a PCM model had no significant effect ($\Delta\Delta E_{zpe}$ < 3 kJ mol^{-1} for the reaction and <3.3 kJ mol^{-1} for individual reactants), we further resigned from using a solvation model. Molecular structures were first energy optimized without symmetry constraints using the XRD data as starting points. Harmonic frequencies and zero-point energies (ZPE) at optimized gas phase structures were calculated at the same levels and showed all molecular geometries to present local minima (only positive eigenvalues of the Hessian matrix) on the potential energy surface. Energies (including vibrational zero-point correction), enthalpies, and free enthalpies calculated for the dissociation reactions are corrected for basis set superposition errors (BSSE), the necessary corrections being obtained by counterpoise calculations. Computations on $\mathbf{10}^+$/$\mathbf{10}^\bullet$ were carried out at the B3LYP/(aug)-cc-pVDZ and CCSD/(aug)-cc-pVDZ levels; both approaches gave similar results, and only the CCSD results will be discussed. MOLDEN[26] and GABEDIT[27] were used for visualization, and NPA spin densities were computed with the program AOMIX.[28]

Acknowledgements

We the bw-grid project[29] for computational resources and Dr W. Frey (Institute of Organic Chemistry, University of Stuttgart) for the collection of X-ray data sets.

Notes and references

1 P. P. Power, *J. Organomet. Chem.*, 2004, **689**, 3904.
2 For reviews on this topic, see: (*a*) P. P. Power, *Chem. Rev.*, 2003, **103**, 789; (*b*) C. D. Martin, M. Soleilhavoup and G. Bertrand, *Chem. Sci.*, 2013, **4**, 3020.
3 M. J. S. Gynane, A. Hudson, M. F. Lappert, P. P. Power and H. J. Goldwhite, *Chem. Soc., Chem. Commun.*, 1976, 623.
4 (*a*) M. J. S. Gynane, A. Hudson, M. F. Lappert, P. P. Power and H. Goldwhite, *Dalton Trans.*, 1980, 2428; (*b*) B. Cetinkaya, A. Hudson, M. F. Lappert and H. Goldwhite, *J. Chem. Soc., Chem. Commun.*, 1982, 609; (*c*) J.-P. Bezombes, P. B. Hitchcock, M. F. Lappert and J. E. Nycz, *Dalton Trans.*, 2004, 499; (*d*) J.-P. Bezombes, K. B. Borisenko, P. B. Hitchcock, M. F. Lappert, J. E. Nycz, D. W. H. Rankin and H. E. Robertson, *Dalton Trans.*, 2004, 1980; (*e*) A. Dumtrescu, V. L. Rudzench, V. D. Romanenko, A. Mari, W. W. Schoeller, D. Bourissou and G. Bertrand, *Inorg. Chem.*, 2004, **43**, 6546; (*f*) P. Agarwal, N. A. Piro, K. Meyer, P. Müller and C. C. Cummins, *Angew. Chem., Int. Ed.*, 2007, **46**, 3111; (*g*) R. Edge, R. J. Less, E. J. L. McInnes, K. Müther, V. Naseri, J. M. Rawson and D. S. Wright, *Chem. Commun.*, 2009, 1691; (*h*) S. Ishida, F. Hirakawa and T. Iwamoto, *J. Am. Chem. Soc.*, 2011, **133**, 12968; (*i*) O. Back, B. Donnadieu, M. van Hopffgarten, S. Klein, R. Tonner, G. Frenking and G. Bertrand, *Chem. Sci.*, 2011, **2**, 858; (*j*) N. A. Giffin, A. D. Hendsbee, L. L. Roemmele, M. D. Lumsden, C. C. Pye and J. D. Masuda, *Inorg. Chem.*, 2012, **51**, 837; (*k*) D. Förster, H. Dilger, F. Ehret, M. Nieger and D. Gudat, *Eur. J. Inorg. Chem.*, 2012, 3989; (*l*) O. Puntigam, D. Förster, N. A. Giffin, S. Burck, J. Bender, F. Ehret, A. D. Hendsbee, M. Nieger, J. D. Masuda and D. Gudat, *Eur. J. Inorg. Chem.*, 2013, 2041.
5 For a persistent phosphanyl radical stabilised by bulky aryl and phosphanyl groups see: (*a*) M. Cattani-Lorente and M. Geoffroy, *J. Chem. Phys.*, 1989, **91**, 1498; (*b*) S. Loss, A. Magistrato, L. Cataldo, S. Hoffmann, M. Geoffroy, U. Röthlisberger and H. Grützmacher, *Angew. Chem., Int. Ed.*, 2001, **40**, 723.
6 (*a*) S. L. Hinchley, C. A. Morrison, D. W. H. Rankin, C. L. B. Macdonald, R. J. Wiacek, A. H. Cowley, M. F. Lappert, G. Gundersen, J. A. C. Clyburne and P. P. Power, *Chem. Commun.*, 2000, 2045; (*b*) S. L. Hinchley, C. A. Morrison, D. W. H. Rankin, C. L. B. Macdonald, R. J. Wiacek, A. Voigt, A. H. Cowley, M. F. Lappert, G. Gundersen, J. A. C. Clyburne and P. P. Power, *J. Am. Chem. Soc.*, 2001, **123**, 9045.
7 K. B. Borisenko and D. W. H. Rankin, *Inorg. Chem.*, 2003, **42**, 7129.
8 J.-D. Guo, S. Nagase and P. P. Power, *Organometallics*, 2015, **34**, 2028.
9 W. Kutzelnigg, *Angew. Chem., Int. Ed. Engl.*, 1984, **96**, 262.
10 H. R. G. Bender, E. Niecke, M. Nieger and H. Westermann, *Z. Anorg. Allg. Chem.*, 1994, **620**, 1194.
11 R. Grubba, Ł. Ponikiewski, J. Chojnacki and J. Pikies, *Acta Crystallogr., Sect. E: Struct. Rep. Online*, 2009, **65**, o2214.
12 S. Stoll and A. Schweiger, *J. Magn. Reson.*, 2006, **178**, 42; G. R. Eaton, S. S. Eaton, D. P. Barr and R. T. Weber, in *Quantitative EPR – A practitioner's guide*, Springer, Wien, 2010.
13 (*a*) K. Kitaura and K. Morokuma, *Int. J. Quantum Chem.*, 1976, **10**, 324; (*b*) T. Ziegler and A. Rauk, *Inorg. Chem.*, 1979, **18**, 1558.
14 K. S. Kim, S. Karthikeyan and N. J. Singh, *J. Chem. Theory Comput.*, 2011, **7**, 3471.
15 R. Robiette, V. K. Aggarwal and J. N. Harvey, *J. Am. Chem. Soc.*, 2007, **129**, 15513.
16 (*a*) A. Finch, A. Hameed, P. J. Gardner and N. Paul, *J. Chem. Soc. C*, 1969, 391; (*b*) A. A. Sandoval, H. C. Moser and R. W. Kiser, *J. Phys. Chem.*, 1963, **67**, 124; (*c*) F. E. Saalfeld and H. J. Svec, *Inorg. Chem.*, 1964, **3**, 1442; (*d*) N. N. Grishin, G. M. Bogolyubov and A. A. Petrov, *J. Gen. Chem. USSR*, 1968, **38**, 2595; (*e*) C. S. Dean, A. Finch,

P. J. Gardner and D. W. Payling, *J. Chem. Soc., Faraday Trans.*, 1973, 1921.

17 Reviews on phosphenium ions: (*a*) A. H. Cowley and R. A. Kemp, *Chem. Rev.*, 1985, **85**, 367; (*b*) M. Sanchez, M. R. Mazières, L. Lamandé and R. Wolf, *Multiple Bonds and Low Coordination Chemistry in Phosphorus Chemistry*, ed. M. Regitz and O. J. Scherer, Thieme, Stuttgart, 1990, p. 129ff; (*c*) D. Gudat, *Coord. Chem. Rev.*, 1997, **163**, 71; (*d*) H. Nakazawa, *Adv. Organomet. Chem.*, 2004, **50**, 107; (*e*) L. Rosenberg, *Coord. Chem. Rev.*, 2012, **256**, 606.

18 D. Gudat, *Eur. J. Inorg. Chem.*, 1998, 1087.

19 H. H. Karsch, in *Synthetic Methods of Organometallic and Inorganic Chemistry*, ed. G. Brauer and W. W. Herrmann, Thieme, Stuttgart, 1996, vol. 3, p. 110.

20 D. J. Dellinger, D. M. Sheehan, N. K. Christensen, J. G. Lindberg and M. H. Caruthers, *J. Am. Chem. Soc.*, 2003, **125**, 940.

21 G. R. Gillette, A. Igau, A. Baceiredo and G. Bertrand, *New J. Chem.*, 1991, **15**, 393.

22 (*a*) G. M. Sheldrick, *Acta Crystallogr., Sect. A: Fundam. Crystallogr.*, 2008, **64**, 112; (*b*) G. M. Sheldrick, *Acta Crystallogr., Sect. C: Cryst. Struct. Commun.*, 2015, **71**, 3; (*c*) S. Parsons, H. D. Flack and T. Wagner, *Acta Crystallogr., Sect. B: Struct. Sci.*, 2013, **69**, 249.

23 M. J. Frisch, G. W. Trucks, H. B. Schlegel, G. E. Scuseria, M. A. Robb, J. R. Cheeseman, G. Scalmani, V. Barone, B. Mennucci, G. A. Petersson, H. Nakatsuji, M. Caricato, X. Li, H. P. Hratchian, A. F. Izmaylov, J. Bloino, G. Zheng, J. L. Sonnenberg, M. Hada, M. Ehara, K. Toyota, R. Fukuda, J. Hasegawa, M. Ishida, T. Nakajima, Y. Honda, O. Kitao, H. Nakai, T. Vreven, J. A. Montgomery Jr., J. E. Peralta, F. Ogliaro, M. Bearpark, J. J. Heyd, E. Brothers, K. N. Kudin, V. N. Staroverov, R. Kobayashi, J. Normand, K. Raghavachari, A. Rendell, J. C. Burant, S. S. Iyengar, J. Tomasi, M. Cossi, N. Rega, J. M. Millam, M. Klene, J. E. Knox, J. B. Cross, V. Bakken, C. Adamo, J. Jaramillo, R. Gomperts, R. E. Stratmann, O. Yazyev, A. J. Austin, R. Cammi, C. Pomelli, J. W. Ochterski, R. L. Martin, K. Morokuma, V. G. Zakrzewski, G. A. Voth, P. Salvador, J. J. Dannenberg, S. Dapprich, A. D. Daniels, Ö. Farkas, J. B. Foresman, J. V. Ortiz, J. Cioslowski and D. J. Fox, *GAUSSIAN 09 (Revision B01)*, Gaussian, Inc., Wallingford CT, 2009.

24 J.-D. Chai and M. Head-Gordon, *Phys. Chem. Chem. Phys.*, 2008, **10**, 6615.

25 Y. Zhao and D. G. Truhlar, *Theor. Chem. Acc.*, 2008, **120**, 215.

26 G. Schaftenaar and J. H. Noordik, *J. Comput.-Aided Mol. Des.*, 2000, **14**, 123.

27 A. R. Allouche, *J. Comput. Chem.*, 2011, **32**, 174.

28 (*a*) S. I. Gorelsky and A. B. P. Lever, *J. Organomet. Chem.*, 2001, **635**, 187; (*b*) S. I. Gorelsky, *AOMix: Program for Molecular Orbital Analysis*, University of Ottawa, 2012, http://www.sg-chem.net/.

29 bwGRiD (http://www.bw-grid.de), member of the German D-Grid initiative, funded by Federal Ministry for Education and Research and the Ministry for Science, Research and Arts, Baden-Württemberg.